AIAA-2000-3187
Modeling the Effects of Velocity Coupling on the Global Dynamics of Combustion Chambers

Giorgio C. Isella, California Institute of Technology, Pasadena, CA
Fred E. C. Culick, California Institute of Technology, Pasadena, CA

36th AIAA/ASME/SAE/ASEE Joint Propulsion Conference and Exhibit

July 16-19, 2000 Huntsville, AL

Modeling the Effects of Velocity Coupling on the Global Dynamics of Combustion Chambers

G. Isella[1] and F.E.C. Culick[2]
Mechanical Engineering and Jet Propulsion
California Institute of Technology
Pasadena, CA 91125
Tel: (626) 395-4783

Abstract - Considerable data exists suggesting that the response functions for many solid propellants tend to have higher values, in some ranges of frequencies, than predicted by the conventional QSHOD theory.

It is a familiar idea that such behavior is associated with dynamical processes possessing characteristic times shorter than that of the thermal wave in the condensed phase. The QSHOD theory, and most of its variants, contains only the dynamics of that process, which normally has a characteristic frequency in the range of a few hundred hertz. Two previous works seeking to correct this deficiency (T'ien, 1972; Lazima and Clavin, 1992) have focused their attention on including the dynamics of the thermal wave in the gas phase. Both include effects of diffusion that complicate the analysis although the second achieves some simplification by applying the ideas of 'activation energy asymptotics'. While their results differ in detail, both works show influences at frequencies higher than those near the broad peak of the response due to the thermal wave.

Recent theoretical work and simulations show that a combustion response function based on simple pressure coupling is not enough to explain the characteristics of the instability observed experimentally. Namely, differences in the shape of the response function fail to reproduce the differences observed experimentally in the characteristics of the limit cycle reached by combustion chambers with propellants of different chemical (or physical) composition.

On the other hand, velocity coupling in the combustion response seems a promising mechanism able to predict the changes in the unstable modes observed experimentally and to produce considerable effect on the shape of the resulting limit cycle. The Baum and Levine model is used as a starting point in the investigation of velocity coupling. Other models, in which the mass burning rate is modified by some function of the velocity, are also investigated through direct time-simulation and by the use of a continuation method.

Modeling of particle damping at high frequency constitutes a serious consideration in the modeling of the interaction of combustion dynamics and chamber acoustics. The effect of particle size distribution is analyzed by considering an experimental particle size distribution.

The ultimate goal of this work is to find a link between the global dynamics of the combustion chamber and small changes in the combustion dynamics, caused by differences in propellant chemical composition or physical characteristics (for example, particle size and distribution).

Response functions are shown for realistic ranges of the chief parameters characterizing the dynamics of the propellant. The results are also incorporated in the dynamical analysis of a small rocket motor to illustrate the consequences of the combustion dynamics for the stability and nonlinear behavior of unsteady motions in a motor.

1 INTRODUCTION

The interaction of the dynamics of the burning of a solid propellant and the global dynamics of the combustion chamber is analyzed by using a model based on a reduced order representation of the system coupled with different models for the solid propellant.

Traditionally, the analysis of the burning of a solid propellant is based on the QSHOD model ([1], [2]), which includes the dynamics of the thermal wave in the solid phase, while treating the gas phase response in a quasi-steady manner. This leads to a model that gives no consideration to dynamical processes with a characteristic time shorter than that of the thermal wave in the solid phase, while experimental data suggest that many solid propellants have a combustion response function with higher values than predicted by QSHOD model.

The natural extension of the QSHOD theory is to include the dynamics of the thermal wave in the gas phase. Two previous works seeking to correct this deficiency (T'ien, 1972, [3]; Lazmi and Clavin, 1992, [4]) have focused their attention on this intent. T'ien's analysis is based on direct numerical integration of the equations describing the temperature, species and velocity evolution in the flame zone of the gas phase. The chemistry is described by a one-step forward chemical reaction, with the reaction rate expressed by an Arrhenius-type expression.

Clavin achieves some simplification by applying the ideas of 'activation energy asymptotics'. While their results differ in detail, both works show influences at

[1] Graduate Research Assistant, Aeronautical Engineering
[2] Richard L. and Dorothy M. Hayman Professor of Mechanical Engineering and Professor of Jet Propulsion
This work was sponsored partly by the California Institute of Technology and partly by the Caltech Multidisciplinary University Research Initiative under ONR Grant No. N00014-95-1-1338, Program Manager Dr. Judah Goldwasser.

frequencies higher than those near the broad peak of the response due to the thermal wave in the solid phase.
The model can be extended further by introducing the dynamics of a surface layer ([13]): it is well known from many observations, both with high speed films and from pictures taken with scanning electron microscopes, that the surface of a burning solid propellant is certainly not smooth and in general contains both liquid and solid particles. For metallized propellants the agglomeration of aluminum drops is an important process affected, for example, by small amounts of impurities or additives. A simple model of the surface layer has been analyzed in [13], and it shows a larger value of the response of the propellant at higher frequency, when compared to the QSHOD approach.

It was shown ([13]) that the representation of the dynamics of the solid propellant by the use of a response function based on pressure coupling only does not justify the experimental observations reporting large variations in the global dynamic response of the chamber to even minimal variation of the propellant composition or physical characteristics (e.g., grain size or distribution).

Previous work ([15][16]) has been done showing that another mechanism, based on velocity coupling, might be of extreme importance in explaining such behavior. In [15], the authors introduce a model based on nonlinear velocity coupling to explain the observed experimental result of pulsed instabilities, and are able to match experimental results by varying the parameter representing the relative weight of the velocity coupling terms. In [16] the same model is used and global dynamics is investigated by using a solution-continuation method.

The first section of the present paper reviews the governing equations for the whole system and presents a simple framework in which phenomenological modeling of the surface layer can be introduced in the general model considering thermal waves in both the gas and solid phases. The modeling of the surface is based on thermal analysis of the layer and matching of the boundary conditions on the solid and gas-phase side ([13]). No chemical reactions (except for decomposition, based on the Arrhenius law) are considered in either solid phase or surface layer. The response function characterizing the behavior of the system is derived by considering small harmonic oscillations and by linearizing the equations describing the different sections of the propellant.

The problem of including condensed material in the model is analyzed and some of the consequences of using different particle-size distributions are considered. Also velocity coupling, beside pressure coupling, is introduced into the governing equations.

The last part presents some examples and comparisons where the results are incorporated in the dynamical analysis of a small rocket motor to illustrate the consequences of the combustion dynamics for the stability and nonlinear behavior of unsteady motions in a motor. That is part of the primary objective of the Caltech MURI program, to understand the influences of propellant composition and chemistry on the global dynamical behavior of a solid rocket combustor by connecting the microscopic and macroscopic through the response function.

2 GOVERNING EQUATIONS

2.1 Global Dynamics

The analysis is based on the method of modal decomposition and averaging, thoroughly presented in [10]. A wave equation for the pressure in the chamber is derived:

$$\nabla^2 p' - \frac{1}{\bar{a}^2}\frac{\partial^2 p'}{\partial t^2} = h \qquad \hat{n}\cdot\nabla p' = -f \tag{1}$$

where p is chamber pressure, $\bar{a}$ is the speed of sound, $\hat{n}$ is the normal to the chamber walls, h and f include gasdynamics (linear and nonlinear), combustion properties of the propellant and other processes.
The pressure is then expanded as the sum of the acoustic modes of the chamber; this procedure yields a set of coupled ordinary differential equations that can be integrated numerically:

$$\ddot{\eta}_n + \omega_n^2 \eta_n = F_n \tag{2}$$

where:

$$F_n = -\frac{\bar{a}^2}{\bar{p}E_n^2}\left\{\iiint h\psi_n dV + \oiint f\psi_n dS\right\} \tag{3}$$

$$E_n^2 = \int \psi_n^2 dV \tag{4}$$

ψ_n is the function representing the mode shape and η_n is the time-dependent mode amplitude for mode n.

Form (3) is particularly convenient to introduce the contribution due to the burning of the solid propellant, which appears as a surface term:

$$\oint \bar{\rho}\frac{\partial u'}{\partial t}\cdot\hat{n}\psi_n dS \tag{5}$$

where u' is the oscillating velocity, which can also be expressed in terms of the modal expansion used for the pressure.

2.2 Propellant Dynamics

The modeling of propellant combustion typically leads to a result in the form of mass flux from the burning surface. This can be re-written in terms of the unsteady velocity by a simple manipulation ([10]) and introduced directly into (5).

The basic modeling of propellant combustion is based on the thermal equations written for the solid phase, the surface and the gas-phase. Some results relative to this approach are presented in [13], where the global response using pressure coupling is analyzed in detail.

The problem is reduced to one dimension. The definition of the coordinate system is shown in Figure 1. The x axis has the origin always fixed to the propellant surface, the boundary between solid and surface layer. Hence solid material flows from the left at the rate $r = r(t)$, not the average burning rate often assumed. Reduction to a one-dimensional formulation implies an averaging in transverse planes not examined here.

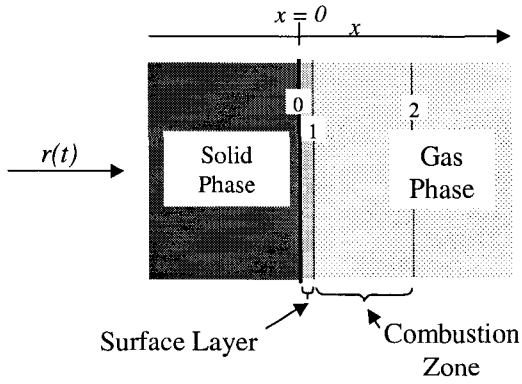

Figure 1. Coordinate definition.

For the purpose of the analysis, the system can be divided into four different regions:

1. Solid phase: $x = (-\infty, 0)$.
2. Surface layer: $x = (0, x_1)$.
3. Gas phase, combustion zone: $x = (x_1, x_2)$.
4. Gas phase, containing products of combustion: $x = (x_2, \infty)$

A set of conservation equations is written for each region, and the boundary values are suitably matched.

The propellant in the solid phase (from $x = -\infty$ to $x = 0$) is assumed to be homogeneous with no chemical reactions. The energy equation for the temperature, written in non-dimensional form is:

$$\rho_c \frac{\partial T}{\partial t} + r(t)\frac{\partial T}{\partial x} - \chi_c \frac{\partial^2 T}{\partial x^2} = 0 \qquad (6)$$

Where the non-dimensional quantities are defined with respect to the quantities in the non-reacting gas phase as ($x \to \infty$):

$$\rho_c = \frac{\rho_c^*}{\rho_\infty^*} \quad T = \frac{T^*}{T_\infty^*} \quad r = \frac{r^*}{\bar{r}^*} \quad t = t^* \frac{\rho_\infty^* C_p u_\infty^2}{k_\infty}$$

$$x = x^* \frac{\rho_\infty^* C_p u_\infty}{k_\infty} \quad \chi_c = \frac{C_p k_c}{C_c k_\infty} \qquad (7)$$

and k is the thermal conductivity; the subscript c refers to the condensed phase, while the subscript ∞ refers to the gas-phase.

Note that the caloric properties of the propellant have been assumed to be uniform and constant.

For the purpose of linear analysis, in the limit of small amplitude oscillations, the variables can be split into the sum of average values and much smaller fluctuating parts, i.e., for the temperature: $T = \bar{T} + \tilde{T}$. Correspondingly, the equations can be written for the steady and unsteady part of the solution.

The boundary conditions for equation (6) are (in non-dimensional form):

For $x \to -\infty$, i.e. at the "cold end" of the propellant: $\bar{T}\big|_{x\to-\infty} = T_0$ and the oscillating temperature $\tilde{T} = 0$.

For $x = 0$ the boundary condition is set by the energy balance at the surface:

$$\left.\frac{\partial T}{\partial x}\right|_{0^-} = \chi_{sl}\left.\frac{\partial T}{\partial x}\right|_{0^+} - \chi_{sl} r L_{c-sl} \qquad (8)$$

where χ_{sl} is the ratio of thermal conductivity of the propellant in the solid phase ($x < 0$) and conductivity of the gas phase; L_{c-sl} is the non-dimensional latent heat $\left(\frac{L^*}{C_p T_\infty^*}\right)$ of the phase transformation between solid and the state in the surface layer. Note that no assumption is made so far concerning the state of the surface layer: it can still be a solid state in a different crystalline form or a liquid film. Whatever chemical transformation takes place between the solid-phase propellant and the surface layer, we assume that it can be described as a chemical change according to the Arrenhius law. In non-dimensional variables, the law can be written as:

$$r = e^{-E_c\left(\frac{1}{T_1} - \frac{1}{\bar{T}_1}\right)} \qquad (9)$$

Note that in (9) we neglect the direct dependence on pressure and temperature; this is justified by the fact that the phase transition from solid state is relatively independent of pressure and temperature. This assumption is also common in the literature ([3], [4]).

The solution to the steady part of (6) for the average temperature ($\bar{T}$) is:

$$\bar{T} = T_0 + \left(\bar{T}_1 - T_0\right)e^{\frac{x}{\chi_c}} \qquad (10)$$

The equation for the fluctuating temperature ($\tilde{T}$) is:

$$\rho_c \frac{\partial \tilde{T}}{\partial t} + r\frac{\partial \tilde{T}}{\partial x} - \chi_c \frac{\partial^2 \tilde{T}}{\partial x^2} + \tilde{r}\frac{\overline{T}_1 - T_0}{\chi_c} e^{\frac{x}{\chi_c}} = 0 \qquad (11)$$

$$(-\infty < x < 0)$$

Equation (11) can be combined with the unsteady version of (8) and (9) to form an equation for the unsteady temperature. Assuming oscillatory solutions (i.e. $\tilde{T} = \hat{T}e^{i\Omega t}$, etc.; Ω is the non-dimensional frequency) and imposing the specified boundary values, it is possible to obtain a relationship between the temperature and the temperature gradient at the surface of the solid phase ($x = 0$) in the form:

$$\left.\frac{d\hat{T}}{dx}\right|_{0^+} = \frac{\hat{T}(0)}{i\Omega\rho_c\chi_{sl}}\left[(i\Omega\rho_c + \Psi)\frac{1+\sqrt{1+4\chi_c i\Omega\rho_c}}{2\chi_c} - \frac{\Psi}{\chi_c} + i\Omega\rho_c\frac{E_c}{\overline{T}_s^2}L\chi_{sl}\right] = \mathrm{K}(\Omega)\hat{T}(0) \qquad (12)$$

$$(x = 0^+)$$

where:

$$\Psi = \frac{E_c}{\overline{T}_1^2}\frac{\overline{T}_1 - T_0}{\chi_c}$$

This expression will be used as a boundary condition on the left side of the surface layer. Note that if we were to use the quasi-steady approach (QSHOD), in which no intrinsic dynamics is associated with the gas phase (and no surface layer is present), (12) would represent the response of the solid phase. We use this expression as a reference to analyze the effect of including the dynamics of the surface layer in the model. Using the non-dimensional variables defined in (7), the non-dimensional frequency has the following expression:

$$\Omega = \omega\frac{k_c\rho_g}{\overline{m}^2 C_p} \qquad (13)$$

The convention adopted to express the non-dimensional frequency in the literature of QSHOD theory ([1], [2]) often uses the density in the solid phase instead of the gas phase. With the parameter values used in the examples reported here (Table 1), the frequency will be scaled by $\rho_c = 1000$.

Since we assume that there is no active chemical reaction in the surface layer, the species balance is unaltered until the boundary of the surface layer and the gas-phase (boundary *1*, in Figure 1). The mass flux balance at the surface (in non-dimensional form) states:

$$\rho_c r = \rho_{0^+} u \qquad (x = 0) \qquad (14)$$

Rewriting (14) for the unsteady variables, and using equation (9), yields:

$$\hat{m}|_{0^+} - \rho_c\frac{E_c}{\overline{T}_1^2}\hat{T}_0 = 0 \qquad (15)$$

This simply states that the oscillations of the temperature and the mass flux are in phase at the interface *0*.

In general, the dynamics of the surface layer (band *0-1* in Figure 1) can be represented by introducing transfer functions connecting fluctuations of mass flux, temperature and heat transfer at the edges of the zone:

$$\hat{m}_1 = M_{surf}(\Omega)\hat{m}_0$$
$$\hat{T}_1 = T_{surf}(\Omega)\hat{T}_0 \qquad (16)$$
$$\left.\frac{d\hat{T}}{dx}\right|_1 = Q_{surf}(\Omega)\left.\frac{d\hat{T}}{dx}\right|_0$$

The transfer functions appearing in the equations above can be derived directly from experiments or from modeling. Note that by using this representation, the result of the QS formulation can be immediately extended to include the surface layer:

$$\frac{\hat{m}_1}{\overline{m}} = R_p(\Omega)M_{surf}(\Omega)\frac{\hat{p}}{\overline{p}} \qquad (x = x_1) \qquad (17)$$

Generally, to accommodate true dynamical behavior in the surface layer, the functions M_{surf}, T_{surf}, Q_{surf} are complex functions.

In [13], some examples are presented where a thermal model and a time-lag model for the surface layer are analyzed.

The conclusion of the analysis of [13] is presented in Figure 2, where the effect of the physical and chemical characteristics of the surface layer are summarized, for a propellant characterized by the parameters presented in Table 1.

E_c	8.0	T_0	0.15
E_l	4.0	T_1	0.35
ρ_c	1000	T_2	0.40
ρ_l	50	χ_c	1.0
γ	1.2	χ_l	1.0
L_c	0.1122	χ_g	1.0
L_{sl}	0.0025	Q_f	12.5

Table 1. Non-dimensional values ([2], [3], [4], [7]).

In the quasi-steady approach (QSHOD) no intrinsic dynamics is associated with the gas phase, so the response of the solid phase to the heat feedback coming from the combustion zone is the one that creates the characteristic response function with a low frequency peak. In our case, (7) would represent the dynamics of the solid phase (it was shown that the temperature and mass fluctuation solutions only differ by a scale factor). Using the values presented in Table 1 it is possible to plot the solid plus surface layer response (equation 17).

The plots are presented in Figure 2. The axes have been re-scaled so that the convention for the non-dimensional frequency is the common one adopted in [1], [2] (i.e. $\Omega = 1000\ \varpi$), and the value at the origin is *1*.

The effect of the surface layer is to generate a second peak in the response function, at a higher frequency than the peak generated by the solid phase alone, and, for the parameters used here, of higher absolute value. Also, as expected, it reduces the influence of the solid phase resonance: the value of the response at the first peak is lower than the case with solid phase only.

Figure 2 shows the effect of activation energy and density of the surface layer on the response function.

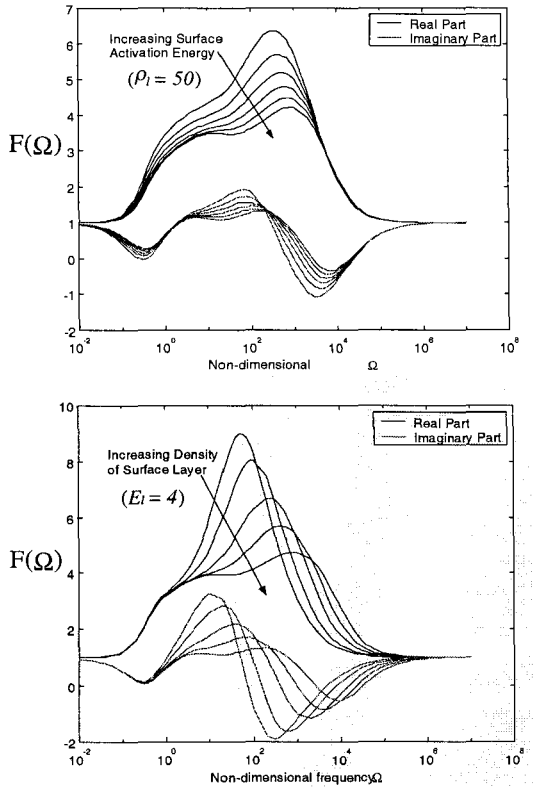

Figure 2. Effect of the activation energy and density on the dynamics of the surface layer.

The peak value of the response function decreases with increasing activation energy and with increasing density of the material composing the surface layer. Note that, as also recalled later, the effect of these propellant changes on the global dynamics is not very relevant.

The same is true for the case of the response calculated including also the dynamics of the gas-phase ([3], [4], [13]). The response function shows larger values at higher frequency with respect to the QSHOD case, but the sensitivity (observed in experiments) of the chamber dynamics to small changes of the propellant is not reproduced by this more complete model of the burning propellant.

2.3 Particle Damping

In [13] it was observed that condensed material in the flow has a significant effect on the global dynamics of the chamber.

The equations representing the dynamics of the chamber (equation 2) can be re-written with the linear contribution explicitly marked:

$$\ddot{\eta}_n + \omega_n^2 \eta_n = 2\alpha_n \dot{\eta}_n + 2\omega_n \vartheta_n \eta_n + (F_n)^{NL} \quad (18)$$

where α_n and ϑ_n are the (linear) growth rate and frequency shift of mode n. Several factors contribute to these two parameters. In particular: combustion, inert surfaces and condensed material in the flow. In general, combustion drives the response, and its contribution is calculated by using proper response functions. Inert surfaces, particularly the nozzle, have a stabilizing effect, and their effect can be introduced by the use of an appropriate value for the admittance ([10]). Condensed material in the flow also has a stabilizing effect, and also a very strong dependence on frequency.

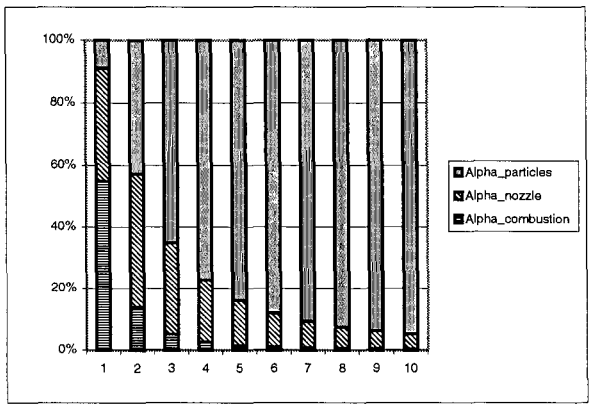

Figure 3. Relative values of contribution to α_n, for fixed particle diameter. First 10 modes.

Figure 3 presents graphically the relative values of the factors contributing to the value of α_n for the first ten modes of the chamber used in the examples of section 3. For clarity, the contributions are presented in their absolute value (α_{Nozzle} and $\alpha_{Particles}$ would be negative). It is clear that, after the second mode, the damping due to the condensed material is dominating the dynamics of the system.

The mechanism responsible for the damping due to condensed material is the viscous interaction between the particles and the gas. Particle damping is calculated by using the linearized multi-component fluid mechanics equations ([10]). Also the assumption is made that the Reynolds number based on the relative speed between

gas and particle is less then unity, and hence Stokes' flow approximation holds.

As it can be expected, the damping is a strong function of the size of the particles and the frequency of oscillation; in particular, the damping at a given frequency presents a maximum at a specific diameter, and, for a given size (within a range, cf. Figure 4), the damping increases greatly with frequency. The situation is summarized in Figure 4.

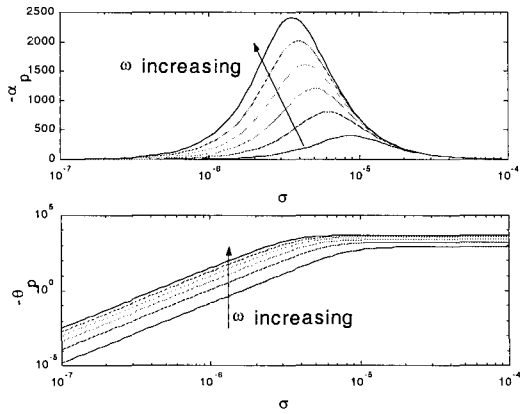

Figure 4. Damping due to condensed material.

Previous calculations ([10], [13]), assumed a constant value ($\sigma = 2x10^{-6}\ m$) for the particle diameter, resulting, as Figure 3 and Figure 4 show, in a very large damping in the high frequency modes.

In [13] it was noticed that an artificial reduction of the particle damping (10% constant reduction over the entire frequency range) could have a significant effect on the global dynamics of the combustion chamber. To investigate further this possibility, we considered introducing a realistic distribution of particle sizes in the calculation. In [14] the author finds that, for a typical aluminized propellant, about 65% of the particles has a diameter between 0.2 and 1 μm ($1x10^{-6}m$), 10% is between $1\mu m$ and 10 μm, the remaining 25% is almost entirely between $10\mu m$ and $30\mu m$, with a few particle (0.02%) falling outside of the categories listed.

Introducing this distribution in the model used to calculate condensed material damping, we obtain the curves presented in Figure 5. The dotted line presents the damping in the case of fixed particle diameter (σ = 2 μm) and the continuous line shows the damping corresponding to the particle distribution measured in [14]. Note that the particle diameter distribution is slightly bimodal, and this is reflected by the two peaks in the damping curve. Note also that, while for the first mode the damping is higher, the particle damping associated with the higher modes is noticeably lower. For reference, in the example presented later, $\omega_1=5.6x10^3$, and $\omega_6=3.4x10^4$.

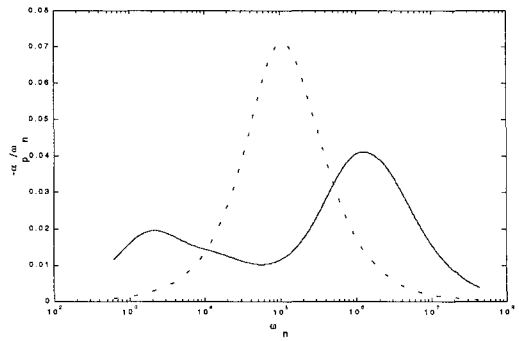

Figure 5. Condensed material damping with variable particle size (continuous line) and constant particle diameter (dotted line) $\sigma=2\mu m$.

With this model, the relative influence of the various components of the growth rate of the modes becomes the one presented in Figure 6 (to be compared with Figure 3).

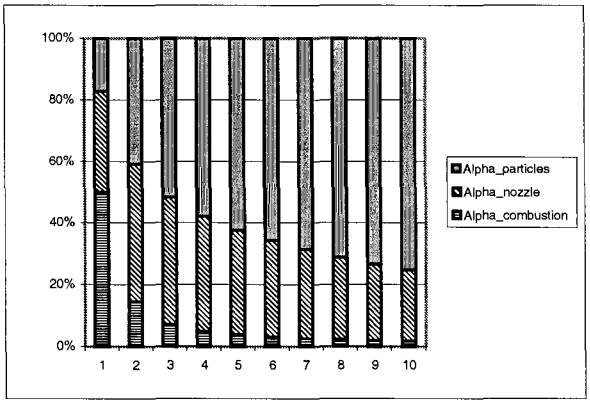

Figure 6. Relative values of contribution to α_n, for distributed particle diameter. First 10 modes.

An example of the calculation of the global response using this model is presented later.

2.4 Velocity Coupling

The idea of velocity coupling is based on the model introduced by Baum and Levine ([15]). The principle is that the velocity parallel to the propellant surface gives a contribution to the mass burning rate of the propellant. This can be justified by the convective heat transfer, that becomes particularly important if the flow is turbulent.

The total mass burning rate can now be written as:

$$\dot{m} = \dot{m}_{pc}\left\{1 + \tilde{R}_{vc}F(\mathbf{u})\right\} \qquad (19)$$

where $\dot{m}_{pc}$ is the mass flux due to pressure coupling, $\tilde{R}_{vc}$ is a coupling coefficient and $F(\boldsymbol{u})$ is the velocity coupling function.

A simple model is to use the oscillating velocity as coupling function. Neglecting the mean flow velocity, equation (19) becomes:

$$\dot{m} = \dot{m}_{pc}\left(1 + \tilde{R}_{vc}|\mathbf{u}'|\right) \tag{20}$$

This expression can be easily introduced in equation (5) to perform the simulations ([16]).

As also noted in [15] and [16], velocity coupling has a significant effect on the global dynamics of the system.

Similarly to [16], in order to use a method based on solution continuation to study the dynamics of the system, a continuous approximation is introduced in equation (20) to substitute the absolute value. This produces a 'threshold' effect responsible for the incurrence of a subcritical bifurcation, as shown in Figure 7, where α is the growth rate of the first mode.

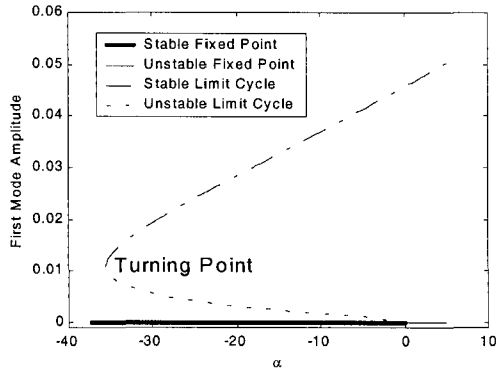

Figure 7. Bifurcation diagram.

In order to analyze the effect of velocity coupling on the overall dynamics, the following two relative sensitivities are defined:

$$S_{\tilde{R}_{vc}}^{A_{LC}} = \frac{1}{A_{LC}}\frac{\partial A_{LC}}{\partial \tilde{R}_{vc}} \tag{21}$$

$$S_{\tilde{R}_{vc}}^{\alpha_{BP}} = \frac{1}{\alpha_{BP}}\frac{\partial \alpha_{BP}}{\partial \tilde{R}_{vc}} \tag{22}$$

where A_{LC} is the amplitude of the limit cycle (defined at a fixed value of α), and α_{BP} is the value of the growth rate at which the unstable fold turns to a stable fold. Equation (21) defines the relative sensitivity of the amplitude of the limit cycle to variations in the velocity coupling coefficient; equation (22) refers to the sensitivity of the turning point to the same coefficient. Figure 8 shows a plot of the sensitivities, calculated for the combustion chamber used in the examples of the following section, and using a six mode approximation of the system. Note that the sensitivity of the turning point is very high, and also the sensitivity of the amplitude of the limit cycle is quite large in the range 0.15 to 0.25 of the coupling coefficient.

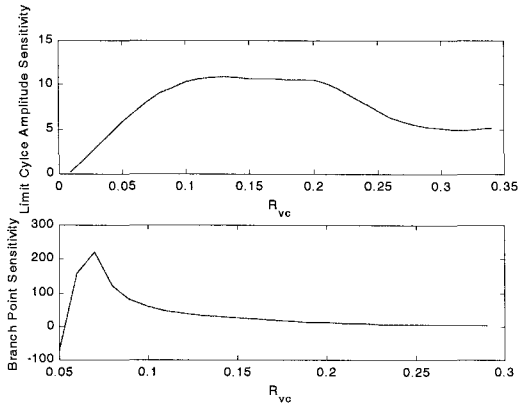

Figure 8. Sensitivity of global dynamics to variations of the coupling coefficient.

3 EXAMPLES

This section presents the dynamical analysis of a small rocket motor to illustrate the consequences of the combustion dynamics for the stability and nonlinear behavior of unsteady motions in a motor. The analysis is based on the method of modal decomposition and averaging, thoroughly presented in [10], and summarized in section 2.1.

The simulated combustion chamber is *0.6 m* long, *0.025 m* in diameter and has a throat radius of *0.009 m*; the mean pressure in the chamber is 1.06×10^7 *Pa*. For reference, Figure 9 presents the results of the simulation for the system with a combustion response based on the quasi-steady theory. The top section presents the combustion response function; the vertical lines mark the non-dimensional frequencies of the acoustic modes of the combustion chamber considered in the simulations. The bottom half shows the time evolution of the amplitude of each mode. The values of the parameters are: $A = 6.0, B = 0.55, n = 0.50$.

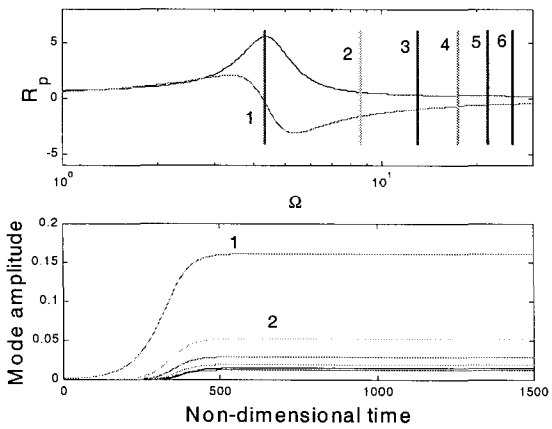

Figure 9. Simulation results for QSHOD combustion response.

The first mode is unstable and rapidly grows to a limit amplitude, while the other modes are all stable, and draw energy from the first mode (allowing the system to enter a limit cycle).

In [13] it was shown that introducing the dynamics of the surface layer and of the gas phase in combustion response functions did not have a very large effect on the overall response of the system (in particular, the amplitude of the limit cycle remains fairly unchanged).

Here we analyze the effect of the velocity coupling, added to the pressure coupling as outlined in section 2.4.

Figure 8 shows that there is a region of high sensitivity of the amplitude of the limit cycle for variations in the velocity coupling coefficient. Figure 10 presents the global response for a small variation of the velocity coupling coefficient ($\tilde{R}_{vc} = 0.15$ and $\tilde{R}_{vc} = 0.165$).

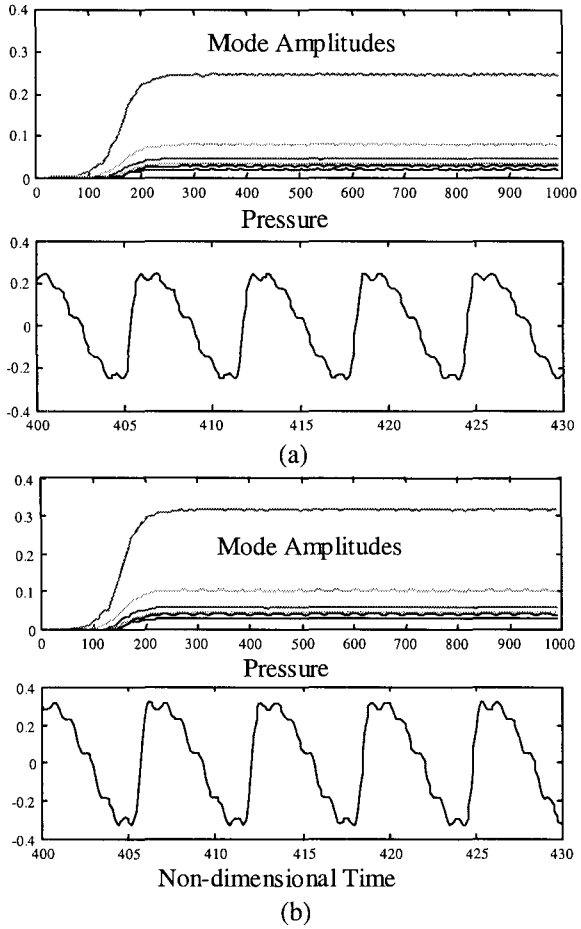

Figure 10. Simulations with velocity coupling for: (a) $\tilde{R}_{vc} = 0.15$, (b) $\tilde{R}_{vc} = 0.165$.

The simulation uses the same coefficients for the pressure coupling as in the results of Figure 9, with the addition of the velocity coupling terms. Figure 11and Figure 12 show the pressure trace and the harmonic content for the same two cases.

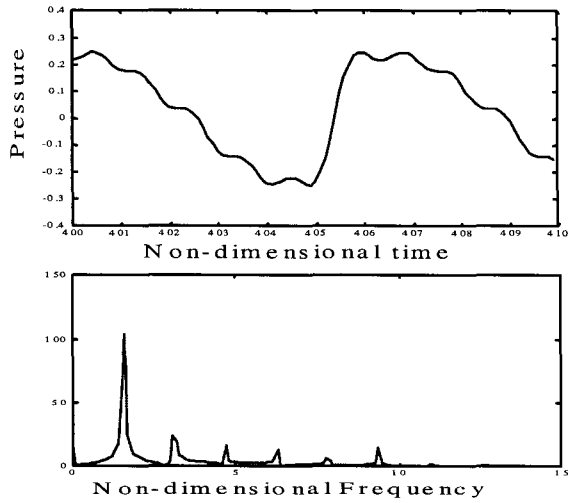

Figure 11. Pressure trace and harmonic content for the case $\tilde{R}_{vc} = 0.15$.

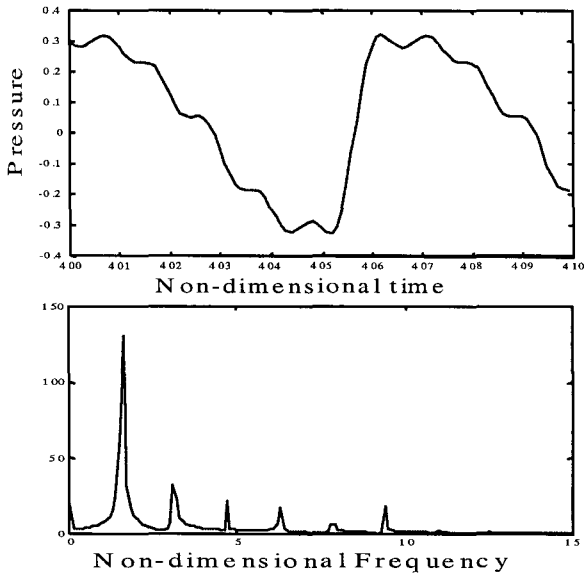

Figure 12. Pressure trace and harmonic content for the case $\tilde{R}_{vc} = 0.165$.

Particle damping has a significant effect on the growth rate of the various modes. Figure 13 shows the same calculation as Figure 10 (a) but with the condensed matter damping calculated according to the particle distribution of [14]. Note the considerably lower value of the limit cycle amplitude, consequence of the fact that the first mode (the unstable one) is more heavily damped. On the other hand, the influence of the higher

frequency modes in the waveform is more pronounced, as clearly shown in Figure 14.

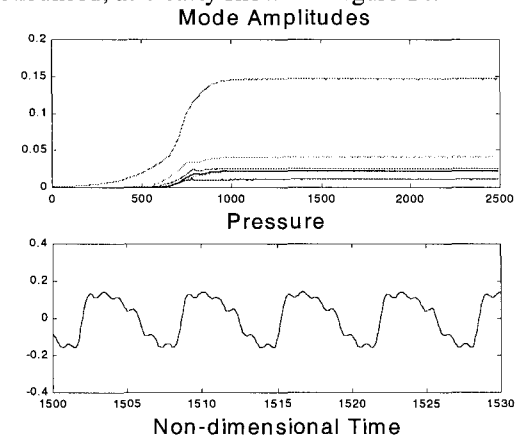

Figure 13. Simulations with particle damping calculated according to the experimental size distribution.

It is interesting to show a result for the response using the combustion response including the surface layer and the gas phase dynamics (as in [13]) and velocity coupling plus the damping model with distributed size (Figure 14).

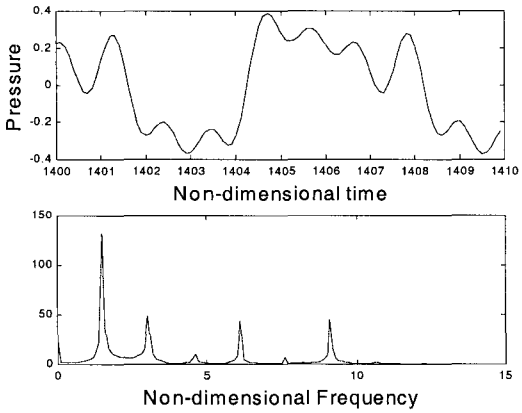

Figure 14. Global dynamics with full combustion response ([13]) and particle damping according to the experimental size distribution.

In this case the first two modes are unstable, and the higher frequency modes are much less damped (due to a combustion response function with higher values than the QSHOD response at high frequency). The result is a higher value of the limit cycle amplitude and a richer harmonic content.

4 CONCLUSIONS

This paper describes a method to relate the dynamics of the burning of a solid propellant to the global dynamics of the combustion chamber. The purpose is to investigate the sensitivity of global dynamics to small changes in the propellant physical and chemical composition.

In [13] it was shown that a model including combustion response based on pressure coupling only is not sufficient to produce large effects in the global dynamics of the system. The only exception is when the combustion response function has values near the boundary for intrinsic stability.

Here the effect of velocity coupling, previously shown to provide the possibility for pulsed nonlinear instabilities, is investigated. The results suggest that unsteady surface combustion responsive to velocity fluctuations parallel to the surface leads to a combustion dynamics sensitive to small compositional changes.

In [13] it was observed that the heavy damping at high frequency, introduced by the model used for condensed matter damping, might have a considerable effect on the global dynamics. More detailed calculations here show that particle damping is effectively an important factor in the simulations; changes in composition of the propellant that would lead to changes in the size (or distribution of sizes) of the condensed material after burning will have a great effect on the global dynamics of the chamber. This is an important point and must be kept into consideration when detailed simulation of combustion chambers is performed.

5 REFERENCES

[1] F. E. C. Culick, *A Review of Calculations for Unsteady Burning of a Solid Propellant*, AIAA Journal, Vol. 6, No. 12, 1968.

[2] M. W. Beckstead, H. B Mathes, E. W. Price, F. E. C. Culick, *Combustion Instability of Solid Propellants*, 12th International Symposium on Combustion, 1969.

[3] J. S. T'ien, *Oscillatory Burning of Solid Propellants including Gas Phase Time Lag*, Combust. Sci. and Tech, 1972, Vol. 5, pp.47-54.

[4] P. Clavin, D. Lazmi, *Theoretical Analysis of Oscillatory Burning of Homogeneous Solid Propellant Including Non-Steady Gas Phase Effects*, Combust. Sci. and Tech., 1992, Vol. 83, pp 1-32.

[5] F. E. C. Culick, G. Isella, C. Seywert, *Influences of Combustion Dynamics on Linear and Nonlinear Unsteady Motions in Solid Propellant Rockets*, AIAA-98-3704.

[6] I-Te Huang, M. M. Micci, *Gas Phase Analysis of Homogeneous Solid Propellant Combustion*, Combust. Sci. and Tech., 1991, Vol. 75, pp. 73-88.

[7] F. E. C. Culick, G. L. Dehority, *An Elementary Calculation for the Burning Rate of Composite Solid Propellants*, Combust. Sci. and Tech., 1969, Vol. 1, pp. 193-204.

[8] F. E. C. Culick, *A Review of Calculations for Unsteady Burning of a Solid Propellant*, AIAA Journal, Vol. 6, No. 12, 1968.

[9] T. Y. Na, *Computational Methods in Engineering Boundary Value Problems*, Academic Press, 1979.

[10] F. E. C. Culick, V. Yang, *Prediction of the Stability of Unsteady Motions in Solid-Propellant Rocket Motors*, in "Nonsteady Burning and Combustion Stability of Solid Propellants", Progress in Aeronautics and Astronautics, Vol. 143, 1992.

[11] H. Grad, *Resonance Burning in Rocket Motors*, Communications in Pure and Applied Mathematics, Vol. 2, March 1949.

[12] S.-I. Cheng, *Unstable Combustion in Solid Propellant Rocket Motors*, Eight Symposium (International) on Combustion, Williams and Wilkins, 1962.

[13] G. Isella, F. E. C. Culick, *Modeling the Combustion Response Function with Surface and Gas Phase Dynamics*, AIAA-2000-0310, AIAA 38th Aerospace Sciences Meeting,*January 10-13, 2000/Reno, NV*

[14] K. J. Kraeutle, *Particle Size Analysis in Solid Propellant Combustion Research*, AIAA, 1978.

[15] J. N. Levine, J. D. Baum, *A numerical Study of Nonlinear Instability Phenomena In Solid Rocket Motors*, AIAA Journal, Vol. 21, No. 4, 1983, pp. 557-564.

[16] V. Burnley, *Nonlinear Combustion Instabilities and Stochastic Sources*, PhD Thesis, California Institute of Technology, 1996.